The Plant Cell, Vol. 25: 4000–4013, October 2013, www.plantcell.org

An ATP Binding Cassette Transporter Is Required for Cuticular Wax Deposition and Desiccation Tolerance in the Moss *Physcomitrella patens*[W]

Gregory J. Buda,[a] William J. Barnes,[a] Eric A. Fich,[a] Sungjin Park,[a] Trevor H. Yeats,[a,1] Lingxia Zhao,[b] David S. Domozych,[c] and Jocelyn K.C. Rose[a,2]

[a] Department of Plant Biology, Cornell University, Ithaca, New York 14853
[b] Plant Biotechnology Research Center, School of Agriculture and Biology, Shanghai Jiao Tong University, Shanghai 200240, China
[c] Department of Biology and Skidmore Microscopy Imaging Center, Skidmore College, Saratoga Springs, New York 12866

ORCID ID: 0000-0003-1881-9631 (J.K.C.R.).

The plant cuticle is thought to be a critical evolutionary adaptation that allowed the first plants to colonize land, because of its key roles in regulating plant water status and providing protection from biotic and abiotic stresses. Much has been learned about cuticle composition and structure through genetic and biochemical studies of angiosperms, as well as underlying genetic pathways, but little is known about the cuticles of early diverging plant lineages. Here, we demonstrate that the moss *Physcomitrella patens*, an extant relative of the earliest terrestrial plants, has a cuticle that is analogous in both structure and chemical composition to those of angiosperms. To test whether the underlying cuticle biosynthetic pathways were also shared among distant plant lineages, we generated a genetic knockout of the moss ATP binding cassette subfamily G (ABCG) transporter Pp-ABCG7, a putative ortholog of *Arabidopsis thaliana* ABCG transporters involved in cuticle precursor trafficking. We show that this mutant is severely deficient in cuticular wax accumulation and has a reduced tolerance of desiccation stress compared with the wild type. This work provides evidence that the cuticle was an adaptive feature present in the first terrestrial plants and that the genes involved in their formation have been functionally conserved for over 450 million years.

INTRODUCTION

The primary interface between a land plant and its aerial environment is provided by the cuticle, a specialized cell wall component produced by epidermal cells that consists of a matrix of the polyester cutin, coated and infiltrated with waxes. Cutin is comprised mainly of hydroxy fatty acids, diacids, and glycerol, whereas waxes can include very-long-chain fatty acids (VLCFAs), primary and secondary fatty alcohols, fatty ketones and aldehydes, alkanes, and wax esters, as well as other non-aliphatic components, such as triterpenoids and flavonoids (Samuels et al., 2008; Javelle et al., 2011). Cutin and waxes are integrated into the outer portion of the polysaccharide cell wall, forming a lipid-impregnated zone known as the cuticular layer (CL), and are also layered on top of the CL to create a hydrophobic surface devoid of polysaccharides called the cuticle proper (CP; Jeffree, 2006).

The cuticle has many functions, perhaps the most critical of which is limiting plant desiccation and regulating water exchange with the surrounding environment (Javelle et al., 2011; Yeats and Rose, 2013). In addition, it serves to separate adjacent organs during their development, acts as a defensive barrier against pests and pathogens (Barthlott and Neinhuis, 1997; Reina-Pinto and Yephremov, 2009), and provides protection from potentially damaging UV radiation (Shepherd and Wynne Griffiths, 2006).

Collectively, these protective roles have led to the suggestion that the development of a cuticle was a key evolutionary adaptation that allowed the first land plants to colonize terrestrial habitats, ~450 million years ago (Wood, 2005; Rensing et al., 2008). The transition to life on land would have necessitated the ability to tolerate a range of abiotic and biotic stresses that would not have been present in exclusively aquatic environments, and the development of a cuticle was likely instrumental in this regard. Numerous reports have described a variety of wax and cutin compositions and cuticle architectural designs across diverse plant taxa (Holloway, 1982; Jetter et al., 2006), and, more recently, many of the genes involved in cuticle precursor biosynthesis, export and assembly have been identified (Javelle et al., 2011; Beisson et al., 2012; Yeats et al., 2012; Yeats and Rose, 2013). However, detailed studies of cuticle biology linking the underlying molecular genetic pathways with composition, structure, and physiological function have mostly focused on experimental model flowering plants, such as *Arabidopsis thaliana* (Javelle et al., 2011), maize (*Zea mays*; Javelle et al., 2011; Post-Beittenmiller, 1998), and tomato (*Solanum lycopersicum*; Leide et al., 2007; Isaacson et al., 2009; Matas et al., 2011). Consequently, there are many unanswered questions that are key to understanding the similarities and differences

[1] Current address: Energy Biosciences Institute, University of California, Berkeley, CA 94720.
[2] Address correspondence to jr286@cornell.edu.
The author responsible for distribution of materials integral to the findings presented in this article in accordance with the policy described in the Instructions for Authors (www.plantcell.org) is: Jocelyn K.C. Rose (jr286@cornell.edu).
[W] Online version contains Web-only data.
www.plantcell.org/cgi/doi/10.1105/tpc.113.117648

between cuticles of diverse and evolutionarily distant plant lineages. For example, is there a common ancestral form of the cuticle in earlier diverging taxa and, if so, are the molecular pathways underlying its biosynthesis and function similar to those of flowering plants? These questions are important for understanding the evolutionary origins of plant cuticles and represent the major focus of this current study.

The bryophytes, comprising the mosses, liverworts, and hornworts, are the extant relatives of the earliest diverging land plants (Rensing et al., 2008). They typically colonize moist habitats and collectively exhibit a range of adaptive strategies to resist or tolerate desiccating conditions, including an abscisic acid–responsive pathway to counter dehydration, accumulation of compatible solutes to retain water, production of rehydrins to prevent cellular damage following rehydration of dry tissues (Charron and Quatrano, 2009), and late embryogenesis abundant protein synthesis (Minami et al., 2005). In addition, there are many reports of cuticles both in early land plants from the fossil record (Jeffree, 2006) and in extant bryophytes (Schönherr and Ziegler, 1975; Caldicott and Eglinton, 1976; Proctor, 1979; Haas, 1982; Sack and Paolillo, 1983; Clayton-Greene et al., 1985; Nissinen and Sewón, 1994; Neinhuis and Jetter, 1995; Budke et al., 2011), though studies of the latter have highlighted chemical composition or architecture, but rarely both.

The moss *Physcomitrella patens* has emerged as a valuable model system to address questions related to bryophyte biology, plant development, and evolution. In addition, *P. patens* has been used extensively for bryophyte genetic studies due to its amenability to genetic modification via homologous recombination (Hohe et al., 2004; Cove et al., 2009). Moreover, following the publication of its genome sequence and the creation of associated functional genomics tools (Rensing et al., 2008), its utility has grown rapidly as a system in which to investigate the evolution of plant gene pathways. For these reasons, this moss represents a potentially excellent system in which to conduct an investigation of the structure, biosynthesis, and function of a putative bryophyte cuticle or equivalent structure. Wyatt et al. (2008) provided preliminary evidence that *P. patens* has a hydrophobic surface layer, but no additional characterization has been described to date. We report here that *P. patens* indeed has a cuticle that is similar in both composition and structure to those of flowering plants and that it shares at least one important cuticle biosynthetic molecular pathway with later diverging plant lineages. In addition, we address the hypothesis that such pathways were likely critical for the early colonization of land through studies of the growth and development of a transgenic *P. patens* line with altered cuticle composition, with particular focus on the effects of exposure to desiccating conditions.

RESULTS

The Phyllids of *P. patens* Are Covered by a Thin and Structurally Simple Cuticle

The dominant phase of the moss life cycle is haploid, unlike flowering plants, and development begins with the germination of a single haploid spore into a network of filamentous protonema (Cove et al., 2006). Protonemal cells can subsequently differentiate to form buds that develop into leafy gametophores. The gametophores of *P. patens* are comprised of leaf-like phyllids, a single cell layer thick, emanating from a central axis (Figures 1A and 1B). After a fertilization event, a sporophyte develops at the apex of a female gametophore shoot, anchored within the gametophyte tissue (Figure 1A). To study the cuticle architecture of *P. patens*, both gametophores and sporophytes were prepared for transmission electron microscopy (TEM) using osmium tetraoxide postfixation to generate image contrast and highlight the lipid components of the cells. A thin cuticle (~50 nm) was observed on both abaxial and adaxial surfaces of the phyllids (Figure 1C) that exhibited similar structural features to those recently described in the moss *Funaria hygrometrica* (Budke et al., 2011). This cuticle can be classified as structural type six, defined by an amorphous CP consisting of an outer osmiophilic layer and an inner electron-lucent layer (Holloway, 1982). The CL is slightly more osmiophilic than the underlying polysaccharide cell wall, with which it is intercalated at the interface (Figure 1C). No apparent structural differences were observed between the abaxial and adaxial phyllid cuticles. Particular attention was paid in preparing the sample to prevent the detachment of the outermost osmiophilic layer of the CP, and only regions of the cell wall where this layer was still attached were selected for imaging. The cuticle of the sporophyte capsule was more substantial (~400 nm), with a highly expanded reticulate region underlying the amorphous and electron-lucent CP (Figures 1D and 1E). The outer periclinal cell walls of the capsule epidermal layer were also much thicker than those of the phyllid epidermis (Figure 1D).

After analyzing the lamellar structure of the cuticle in transverse sections, phyllids were prepared for scanning electron microscopy to determine whether epicuticular wax crystals decorated the surface of the CP, as can often been seen in flowering plants. The gametophores were air dried for several hours prior to sputter coating as this decreased the number of cells that ruptured when the vacuum was applied. Areas with dense, irregularly shaped wax platelets were observed on many phyllids (Figures 2A and 2B), but the presence and density of wax crystals were highly variable between gametophores and phyllids, and even within regions of a single phyllid. Most phyllid epidermal cells exhibited a smooth surface, suggesting an amorphous epicuticular wax film, but when observed, the wax crystals were predominantly in areas over the anticlinal cell walls, as opposed to the center of the cell. Developmental differences in wax accumulation were also noted as wax crystals were more prevalent in older phyllids taken from the base of the gametophores and were not observed on younger phyllids close to the shoot apex.

P. patens Cutin Analysis

Protocols used to evaluate the cuticle composition of *Arabidopsis* (Li-Beisson et al., 2010) were adapted to investigate the chemical constituents of the *P. patens* cuticle. Ground moss colonies were extensively delipidated with a series of organic solvents, and the remaining plant residue was depolymerized by

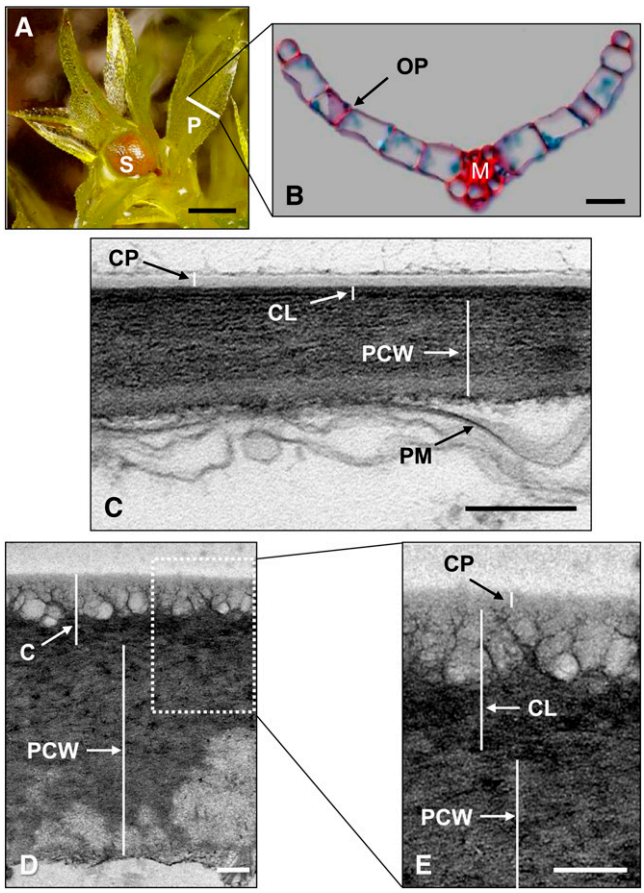

Figure 1. *P. patens* Morphology and Cuticle Structure.

(A) *P. patens* gametophore with several phyllids (P) and an immature sporophyte (S) growing from the apex.
(B) *P. patens* phyllid shown in transverse section, corresponding to the white line in **(A)**, consisting of a single-cell-layer-thick lamina attached to a central midrib (M). Cell walls are stained red and intracellular contents blue. OP, outer periclinal wall.
(C) Transmission electron micrograph of the phyllid outer periclinal cell wall, showing the layers of the cuticle (CL), polysaccharide cell wall (PCW), and plasma membrane (PM).
(D) Transmission electron micrograph of the sporophyte capsule outer periclinal cell wall (cuticle [C]).
(E) Expanded view of the box in **(D)**.
Bars = 750 μm in **(A)**, 20 μm in **(B)**, and 200 nm in **(C)** to **(E)**.

methanolysis to release methyl esters of any cutin monomers prior to analysis using gas chromatography–mass spectrometry (GC-MS). Cutin monomer identity was assigned based on reference to known mass pectra and retention index (Figure 3). The most abundant aliphatic monomer was 5-hydroxytetradecane dioic acid, and substantial amounts of 10,16-dihydroxyhexadecanoic acid were detected, together with lesser amounts of 16-hydroxyhexadecanoic acid. No substituted C_{18} fatty acids or diacids were detected, although a C_{18} triol was identified in minor quantities. Large amounts of phenolic cutin monomers, specifically *m*- and *p*-coumaric acid and caffeic acid, were also identified, although no ferulic acid appeared to be present. Several peaks corresponded to ions resulting from presumed α-cleavage of cutin monomers containing midchain hydroxyl groups. However, the structures from which these were derived could not be conclusively identified, and they were therefore designated as unidentified. Methyl esters of fatty acids were not considered further as they were likely derived from wall-bound lipids, a term that is commonly used to refer to noncuticular lipids that remain in cell wall extracts following cutin depolymerization treatments. Because of the complexity of the sample, we cannot exclude the possibility that other monomers comprising a small percentage of the cutin matrix were present but were not identified or detected due to their low abundance and/or unfamiliar fragmentation patterns.

P. patens Cuticular Wax Analysis

The composition of waxes was determined by chloroform extraction using a single large biological pool containing many thousands of individual moss plants, since the less abundant

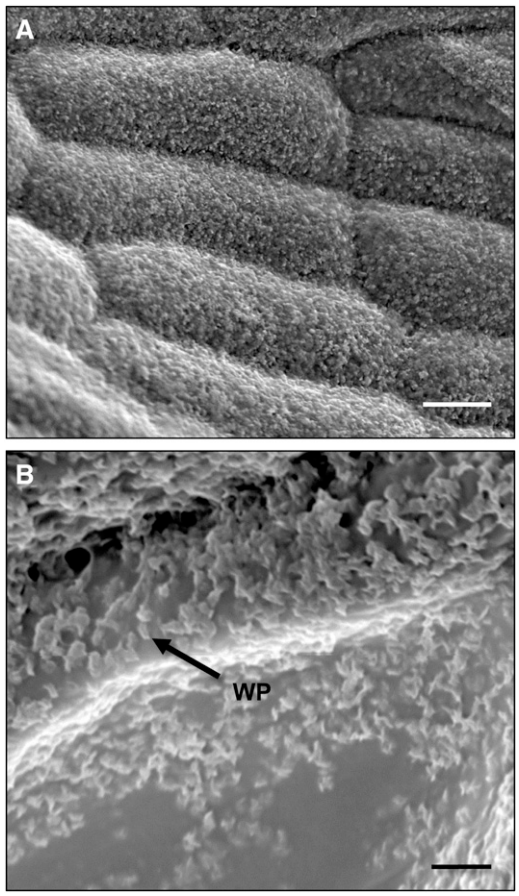

Figure 2. *P. patens* Epicuticular Wax.

(A) Scanning electron micrograph of phyllid epidermal cells densely covered in wax platelets.
(B) Higher magnification scanning electron micrograph showing morphology of wax platelets (WP; arrow).
Bars = 10 μm in **(A)** and 2 μm in **(B)**.

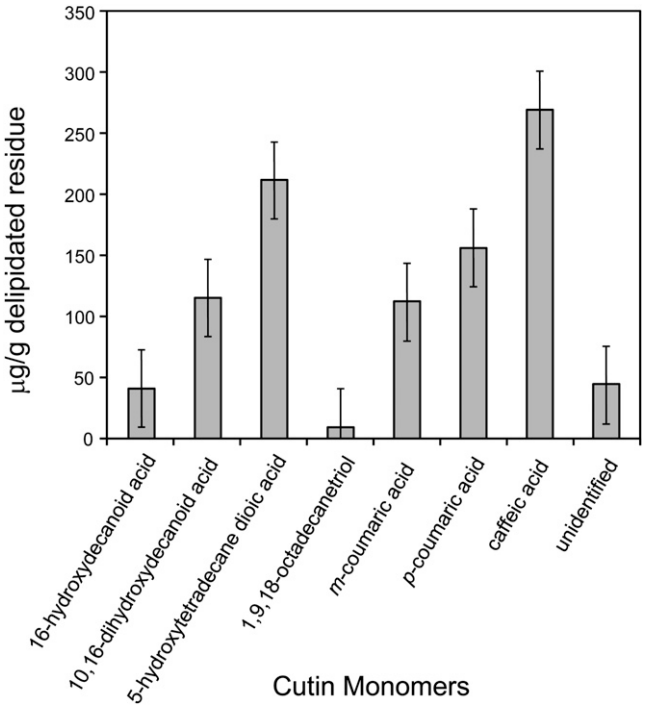

Figure 3. *P. patens* Cutin Monomer Composition and Amount, as Determined by GC-MS.

Error bars indicate SE; $n = 4$.

waxes were consistently below the detection limit in smaller sample sizes. This ensured that the extraction was consistent across all plants but meant that any minor compositional differences between moss colonies or gametophores were not considered. A prefractionation step using thin-layer chromatography (TLC) was included in the analysis to improve the identification and quantification of wax compounds and to reduce deterioration of peak quality during the subsequent GC-MS analysis that occurred when attempting to analyze derivatized crude wax extracts. The major compound classes present were primary fatty alcohols and long-chain wax esters, with minor amounts of VLCFAs and alkanes (Figures 4A to 4D), while secondary fatty alcohols, ketones, or fatty aldehydes were not detected. The additional TLC bands most likely resulted from intracellular lipid contamination and corresponded to triacyl glycerols and steryl esters, which are present in large amounts in gametophyte tissues (Huang et al., 2009).

The distribution of carbon chain length within each wax compound class followed the expected pattern with long-chain wax esters, primary fatty alcohols, and VLCFAs exhibiting a strong bias toward chain lengths with an even number of carbons (Figures 4A to 4C). Conversely, the alkanes, arising from decarbonylation of VLCFAs during their biosynthesis, exhibited an odd chain length bias (Figure 4D). Alkanes shorter than C_{25} were not considered in the survey as they did not exhibit the odd chain length preference characteristic of cuticular alkanes and likely corresponded to contaminants introduced during prefractionation from sources such as plasticware.

Functional Analysis of *ABCG7*, a Putative Moss Wax Transporter Gene

After determining that *P. patens* has a cuticle that is both structurally and compositionally similar to those of flowering plants, we addressed the hypothesis that the basic underlying molecular genetic pathways involved in cuticle formation have also been closely conserved throughout plant evolution. Since *Arabidopsis* has the most comprehensive set of characterized cuticle-associated genes, we used an extensive selection of these to search the *P. patens* genome sequence for putative orthologs. Many candidate genes were identified with a high degree of predicted protein sequence similarity to those known in *Arabidopsis* to be involved in various aspects of wax and cutin biosynthesis and cuticle formation.

One of these, *ABCG7* (Rensing et al., 2008), is predicted to be a 10-exon gene, spanning 3544 bp, and encoding an ABC half transporter in the G subfamily, with 63% amino acid identity and 78% similarity with the *Arabidopsis* protein At-ABCG11 (also named White Brown Complex11 [WBC11]) and slightly lower sequence homology to At-ABCG12 (also named WBC12 and Eceriferum 5; 52% identity and 72% similarity). A phylogenetic analysis of all predicted ATP binding cassette subfamily G (ABCG) half transporters from *Arabidopsis* and *P. patens* revealed that Pp-ABCG7 falls into a well-supported clade containing all of the *Arabidopsis* ABCG half transporters that have previously been shown to be involved in cuticle formation (Figure 5; see Supplemental Data Set 1 online). Of these, At-ABCG11 and At-ABCG12 are two well characterized members that are required for the trafficking of wax and cutin precursors through the plasma membrane and whose loss-of-function mutants show severe abnormal cuticle phenotypes (Pighin et al., 2004; Bird et al., 2007; Luo et al., 2007).

The subcellular localization of Pp-ABCG7 was evaluated by transient coexpression in onion (*Allium cepa*) epidermal cells of full-length Pp-ABCG7 fused to red fluorescent protein (RFP) at the C terminus, together with the plasma membrane resident *Arabidopsis* aquaporin At-PIP2a fused to green fluorescent protein (GFP). Confocal imaging revealed that PpABCG7-RFP and AtPIP2a-GFP showed overlapping expression in plasmolyzed transformed onion cells (see Supplemental Figure 1 online), indicating that Pp-ABCG7 localizes to the plasma membrane, consistent with its putative function as an ABCG half transporter.

To establish whether Pp-ABCG7 has similar functions in trafficking cuticle components, a targeted *ABCG7* knockout mutant was generated. Approximately 1.1 kb of flanking sequence both upstream and downstream of the gene was cloned into the pTN80 vector on either side of the *nptII* G418 resistance marker (Figure 6A). These 5′ and 3′ flanking regions served to target the knockout cassette to the Pp-*ABCG7* gene and allowed replacement with the selectable marker. Wild-type moss protoplasts were transformed as previously described (Cove et al., 2009; Saavedra et al., 2011) via polyethylene glycol–mediated transformation. Transformed protoplasts were regenerated and the resulting moss colonies were subjected to two rounds of selection with the antibiotic G418 to yield a collection of potential stable knockout lines. Each of these lines was

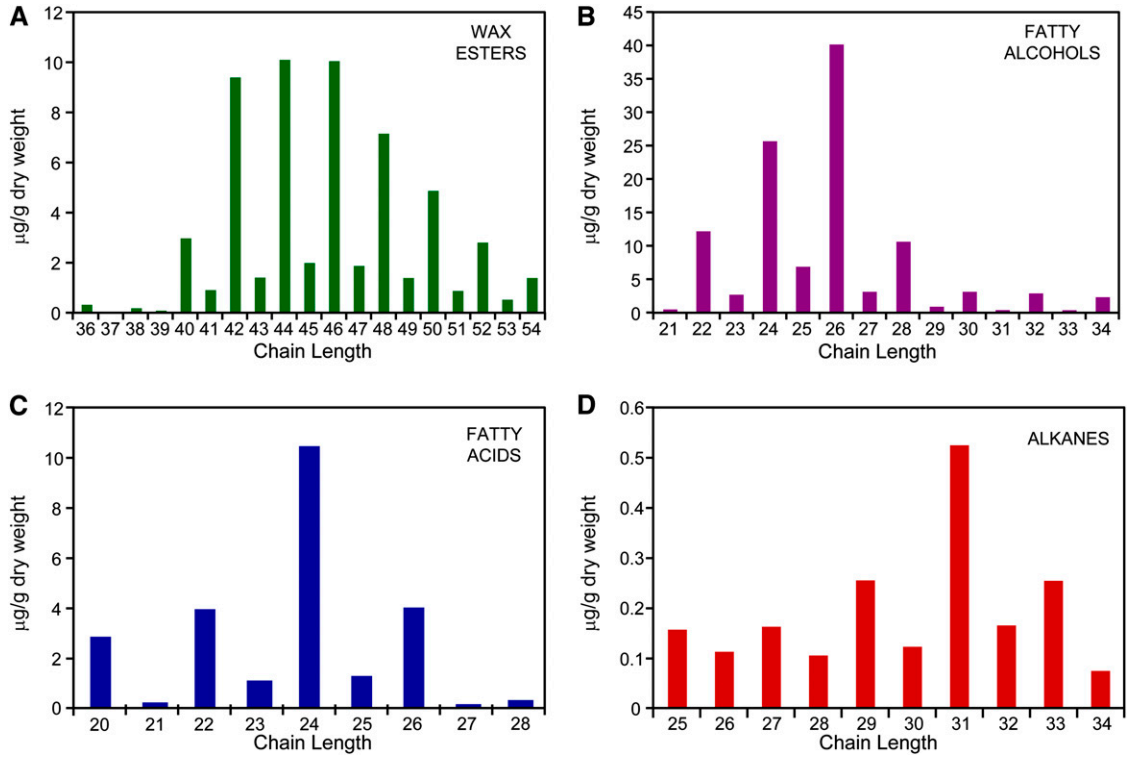

Figure 4. *P. patens* Wax Composition and Amount, as Determined by GC-MS.

Homolog series for wax esters **(A)**, fatty alcohols **(B)**, fatty acids **(C)**, and alkanes **(D)**.

screened using appropriate PCR primers for the absence of Pp-*ABCG7*, presence of the *nptII* selectable marker, and for correct targeting of the selectable marker within the genome (Figures 6A and 6B; see Supplemental Table 1 online). One line was identified as being a correctly targeted, stable knockout of Pp-*ABCG7* and was designated Δ*ppabcg7*. To verify that Pp-*ABCG7* expression was completely abolished in Δ*ppabcg7*, mRNA was extracted from both wild-type and Δ*ppabcg7* protonema and gametophores and used to generate cDNA libraries, which were then screened using PCR primers designed to amplify a 221-bp fragment in the 3′ untranslated region of Pp-*ABCG7* (Figure 6C). The *ABCG7* transcript was detected in the wild-type leafy gametophore tissue but not in the protonemal tissue, which is consistent with the expected expression pattern for a gene involved in cuticle formation, since the *P. patens* protonema lacks a cuticle (Wyatt et al., 2008). However, no expression was detected in either tissue from Δ*ppabcg7*, confirming the absence of *ABCG7* expression in this line.

Δ*ppabcg7* Exhibits Stunted Growth and Altered Spore Wall Architecture

Development of protonemal colonies and initiation of gametophore shoots were similar in Δ*ppabcg7* and the wild type (Figure 7A); however, Δ*ppabcg7* gametophores were ~50 to 75% smaller than the wild type, exhibiting a reduction in both gametophore height and phyllid size (Figures 7A and 7B). In addition, Δ*ppabcg7* colonies had noticeably more rhizoids than wild-type plants (Figure 7B), and sporophytes showing stunted, shriveled, and abnormal development (see Supplemental Figure 2 online). The spores of the wild type and Δ*ppabcg7* also showed distinct differences in their surface decorations: The protrusions of the wild-type spore wall were elongated, evenly spaced, and pointed (Figures 8A and 8B), while those of the Δ*ppabcg7* spore wall were smaller, nonuniform in size, rounded, and more densely packed over the entire surface (Figure 8C). However, despite these structural abnormalities, Δ*ppabcg7* spores were viable.

Δ*ppabcg7* Has a Substantial Reduction in the Levels of Cuticular Wax but Not of Cutin

To determine whether cuticle biosynthesis in Δ*ppabcg7* is perturbed, we evaluated wax and cutin content. Waxes were extracted from large biological pools of either wild-type or Δ*ppabcg7* colonies. The latter showed a dramatic reduction in wax load for all compound classes of surface waxes except alkanes, which were only slightly reduced relative to the wild type (Figure 9A). By contrast, total cutin load was not significantly different compared with the wild type (Figure 9B), and the slight reduction observed can be attributed to lower levels of *m*-coumaric acid and caffeic acid in Δ*ppabcg7.* We note that replicate measurements of surface wax load reduction were not feasible in this study due to the extremely large amounts

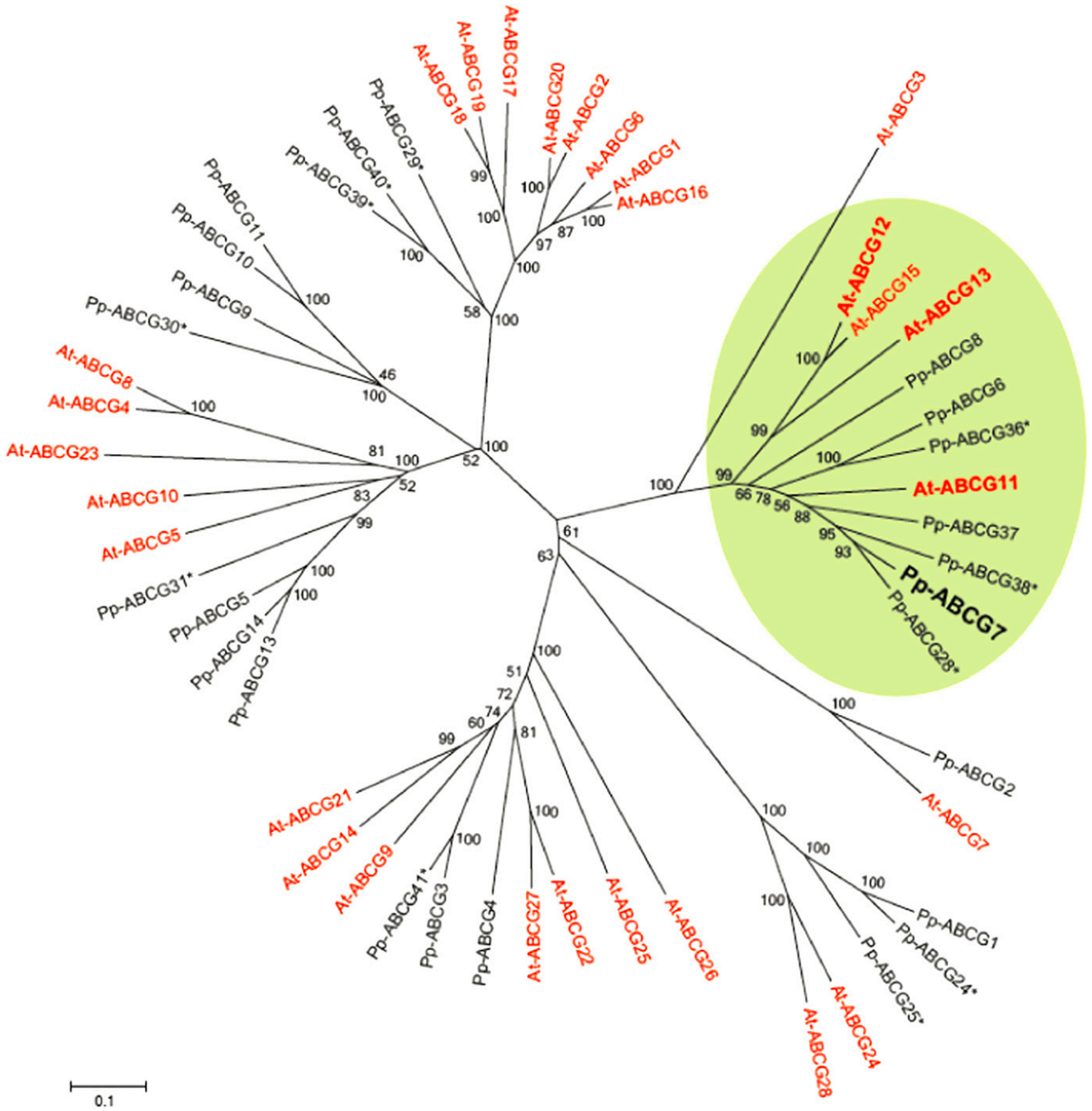

Figure 5. Unrooted Neighbor Joining Protein Phylogeny of Predicted ABCG Half Transporters from *Arabidopsis* and *P. patens*.

Arabidopsis subfamily members are shown in red and *P. patens* subfamily members in black. Those marked by an asterisk are not supported by EST evidence. The clade highlighted by a green background contains all of the *Arabidopsis* ABCG half transporters known to be involved in cuticle precursor export (bold), as well as the putative moss wax transporter Pp-ABCG7. Bootstrap values (1000 replicates) are given for each node. Bar indicates 0.1 amino acid substitutions per site.

of moss material needed. However, the lack of a statistically significant difference in levels of cutin extracted from the same pooled biological samples, for which replicate analyses were performed (Figure 9B), indicates that the differences in waxes were specific and not due to a general reduction in cuticle material or some other artifact induced during sample preparation.

We prepared samples of Δ*ppabcg7* gametophores to examine cuticle structure using TEM and scanning electron microscopy. No noticeable phenotypic differences were observed in the Δ*ppabcg7*

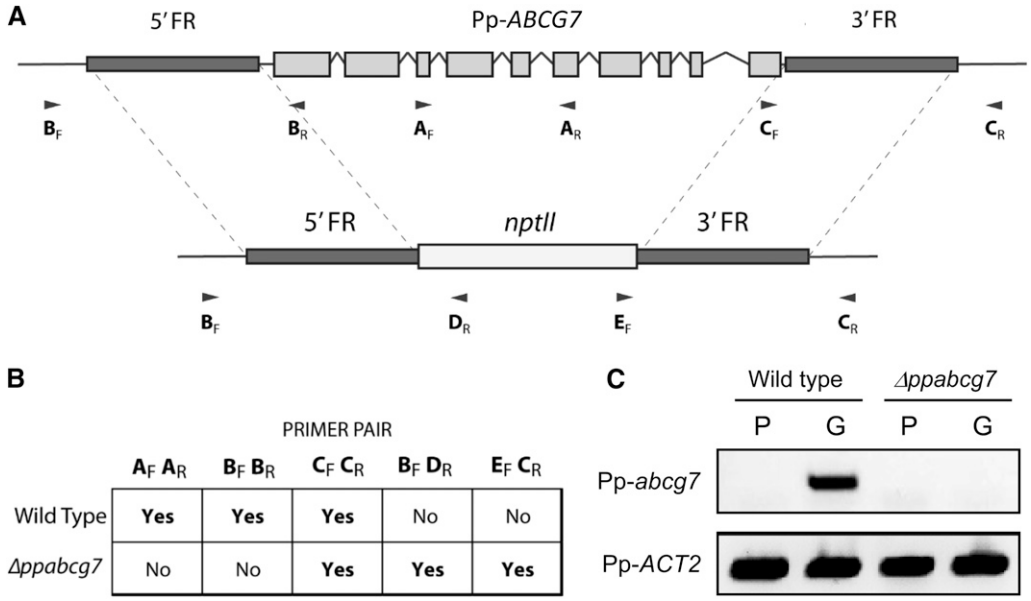

Figure 6. Generation of the Δ*ppabcg7* Knockout Mutant.

(A) Schematic diagram depicting the targeted replacement of Pp-*ABCG7* with the *nptII* selectable marker by homologous recombination to yield a stable *P. patens* knockout mutant. (FR, flanking region).

(B) PCR screening of wild-type and Δ*ppabcg7* genomic DNA with the PCR primer pairs shown in **(A)** showing the presence (Yes) or absence (No) of an amplified product. Primer pairs specific to Pp-*ABCG7* generate a PCR product in the wild type but not in Δ*ppabcg7.*

(C) PCR screening of wild-type and Δ*ppabcg7* cDNA with Pp-*ABCG7* transcript-specific primers, showing that Pp-*ABCG7* expression is abolished in Δ*ppabcg7* (P, protonema; G, gametophore). Primers specific to *P. patens* actin (Pp-*ACT2*) were used as a control for cDNA quality.

cuticle, either in the phyllid or in the sporophyte. Scanning electron microscopy analysis suggested a decrease in the abundance of epicuticular wax crystals on the phyllids, but because their presence was so variable in wild-type phyllids, it was not possible to conclude that there was a reduction in Δ*ppabcg7.* However, while areas containing small crystals were observed in Δ*ppabcg7*, regions with wax crystals as large or populous as those seen in the wild type (Figures 2A and 2B) were not apparent.

Pp-*ABCG7* Does Not Functionally Complement a Mutation in the Homologous *Arabidopsis* Gene *ABCG12*

The substantial reduction in wax levels in Δ*ppabcg7* is reminiscent of a similarly large reduction in waxes reported in the *Arabidopsis abcg12* (*wbc12*) mutant (Pighin et al., 2004), which has perturbed expression of *ABCG12*, a closely related homolog of Pp-*ABCG7* (Figure 5). To investigate whether Pp-*ABCG7* is a functional ortholog of At-*ABCG12*, as the mutant phenotype suggests, transformants of the At-*abcg12* mutant expressing Pp-*ABCG7* driven by the constitutive 35S promoter were generated (see Supplemental Figure 3A online) and the cuticles of the transgenic plants evaluated to determine whether the mutant had been rescued. In wild-type *Arabidopsis*, the 29C alkane accounts for over 50% of the wax load in mature stems (Li-Beisson et al., 2010). This was used as a diagnostic compound to determine whether the complementation was successful. Wax was extracted from the inflorescence stems of T2 plants, some of which carried the transgene and some of which did not, as well as from wild-type Columbia-0 plants and the amount of 29C alkane in each line was determined (see Supplemental Figure 3B online)). The amount of 29C alkane in At-*abcg12* mutant plants was substantially reduced relative to the wild type but was equally low in the Pro35S:PpABCG7 lines, indicating that complementation of the mutation did not occur.

Δ*ppabcg7* Has a Reduced Tolerance of Desiccation Stress

Given the substantially reduced wax load in Δ*ppabcg7*, we hypothesized that this might result in reduced vitality under desiccating conditions. Six-week-old colonies of both the wild type and Δ*ppabcg7* were exposed to atmospheres of different RH and their growth monitored by measuring the fresh weight of the moss on each plate every 3 d over a 21-d period. At 100% RH, both the wild type and Δ*ppabcg7* grew at the same rate (Figure 10A), while at 91% RH, wild-type colonies maintained their original fresh weight for the duration of the experiment but showed no significant growth. However, Δ*ppabcg7* colonies exposed to 91% RH maintained their original fresh weight for only 12 d, before rapidly losing weight and eventually dying (Figure 10B). At 86% RH treatment, both lines steadily lost weight until they were highly desiccated and necrotic (Figure 10C).

DISCUSSION

P. patens Has a Cuticle That Is Architecturally and Compositionally Similar to Those of Later Diverging Land Plants

TEM imaging of the *P. patens* phyllid cell walls revealed a thin cuticle evenly coating the whole phyllid surface, approximately the

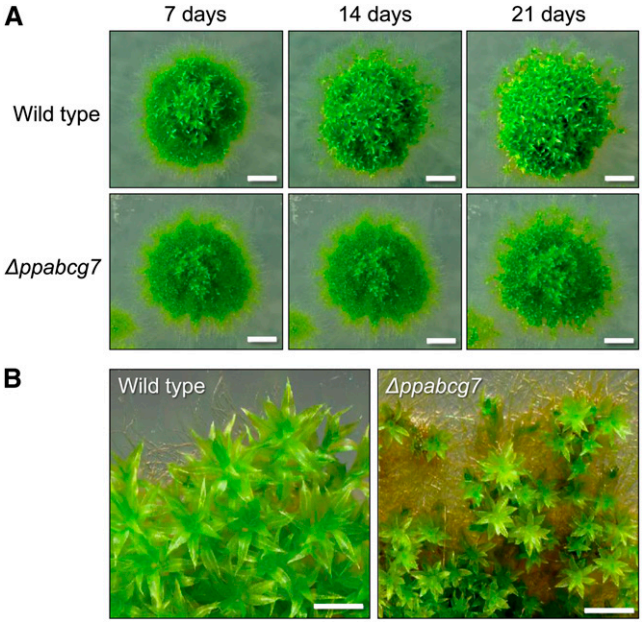

Figure 7. Stunted Growth Phenotype of Δ*ppabcg7*.

(A) Development of wild-type and Δ*ppabcg7* colonies over a 21-d time period showing stunted growth of the Δ*ppabcg7 g*ametophores.
(B) Close-up view of wild-type and Δ*ppabcg7* colonies, showing stunted growth of gametophores in the mutant line.
Bars = 5 mm in **(A)** and 2 mm in **(B)**.

same thickness as that of the *Arabidopsis* leaf cuticle (Figure 1C). Flowering plants are covered by a waterproof cuticle, and gas exchange for photosynthesis is facilitated by stomata that connect the outside environment with internal air spaces. However, bryophytes, other than a few select examples (Sack and Paolillo, 1983; Beerling and Franks, 2009), do not have stomata, and in the case of *P. patens*, the photosynthetic phyllids are only a single cell layer thick (Figures 1A and 1B). Therefore, a cuticle is likely necessary in preventing rapid water loss from phyllid cells, but it must at the same time be sufficiently permeable to allow gas exchange, as no alternate internal routes exist.

Despite the variability of epicuticular wax crystal density (Figure 2) on the phyllids, the predominance of crystals on older phyllids near the base of the gametophores suggests a developmental program for wax synthesis. The substantially thicker cuticle of the sporophyte capsule (Figures 1D and 1E) may reflect the fact that the moss sporophyte is nutritionally depended on the female gametophores to which it is anchored, so a cuticle that is sufficiently permeable to allow gas exchange for photosynthesis is presumably not as important. Furthermore, the water status of the sporophyte capsule must be carefully controlled to ensure spore dispersal under the appropriate conditions (Duckett et al., 2009), which would be facilitated by the presence of a more robust cuticle. Taken together, these results suggest that the elaboration of the cuticle biosynthetic program in the sporophyte generation may have served as the foundation for producing a larger and more complex cuticle in the sporophyte-dominant, later-diverging land plants.

Biochemical analysis resulted in the identification of the major *P. patens* cutin aliphatic monomers as 5-hydroxytetradecanedioic acid (C_{14}), 10,16-dihydroxyhexadecanoic acid (C_{16}), and 16-hydroxyhexadecanoic acid (C_{16}) (Figure 3), revealing clear similarities with the cutin components of diverse plant taxa. Shorter chain length hydroxyalkane diacids (C_{14}-C_{16}) are substantial components of the cutin matrix in a variety of plant species, including *Gnetum gnemon* (Hunneman and Eglinton, 1972) and *Limonia acidissima* (Das and Thakur, 1989), as well as minor components of *Sphagnum* moss (Caldicott and Eglinton, 1976), *Ginkgo* (Hunneman and Eglinton, 1972), and coffee (*Coffea arabica*; Holloway et al., 1972). In some cases, a particular monomer can comprise >80% of the cutin precursor population, such as 10,16-dihydroxyhexadecanoic acid in tomato fruit cutin (Isaacson et al., 2009). We also found minor amounts of 1,9,18-octadecanetriol (C_{18}). Alkanetriols have been shown to be present in large amounts in the cutins of earlier diverging land plants, such as *Psilotum* (Caldicott et al., 1975), suggesting that the incorporation of these monomers into cutins is ubiquitous in land plants.

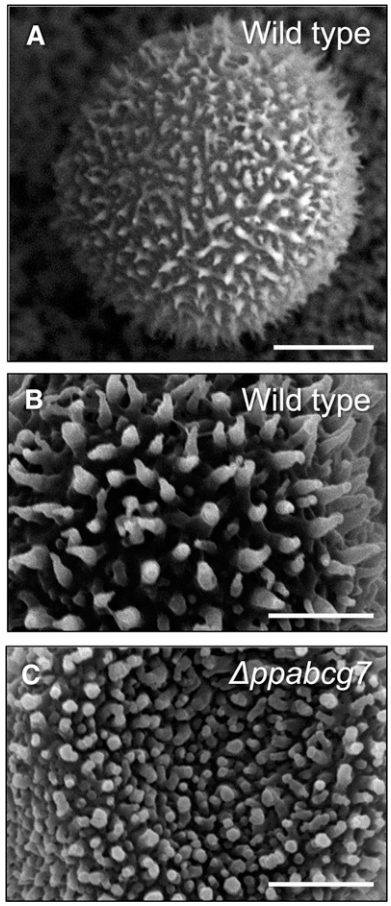

Figure 8. *P. patens* Spore Phenotypic Analysis.

Scanning electron micrographs of spore surface decorations in the wild type (**[A]** and **[B]**) and Δ*ppabcg7* **(C)**, showing irregular and rounded protrusions in the mutant. Bars = 10 μm in **(A)** and 5 μm in **(B)** and **(C)**.

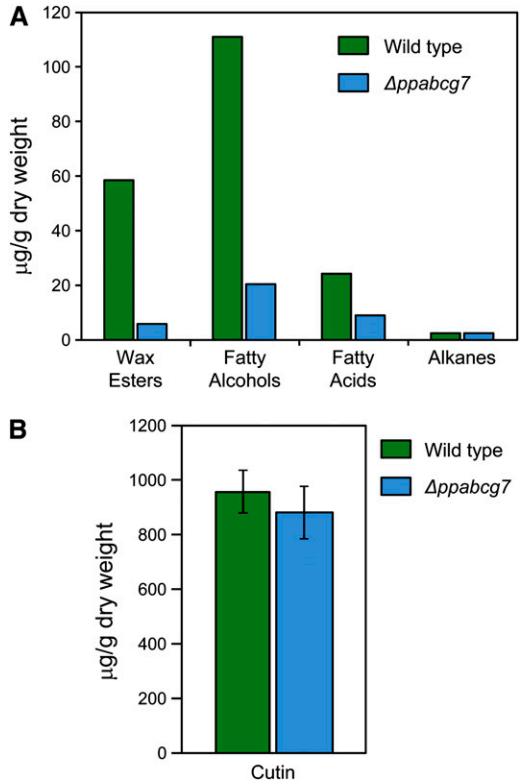

Figure 9. Cuticle Composition Analysis.

(A) Cuticular wax levels in wild-type and Δ*ppabcg7* moss.
(B) Cutin monomer levels in the wild type and Δ*ppabcg7*. Error bars indicate SE; $n = 4$.

A particularly notable result was the high levels of aromatic cutin monomers in *P. patens* cutin, with *m*- and *p*-coumaric acid and caffeic acid (Figure 3), which together account for >50% of the cutin monomers. There has been considerable debate as to whether these aromatic acids are actually incorporated into the cutin matrix (Holloway, 1982), but an *Arabidopsis* acyl-transferase was recently identified that esterifies ferulic acid to ω-hydroxy fatty acids and a loss of function of the corresponding gene results in the absence of ferulate in leaf cutin (Rautengarten et al., 2012). However, this deficiency does not apparently affect permeability of the cuticle to water, suggesting that these aromatic monomers do not significantly contribute to reducing transpirational water loss. The presence of such high amounts in moss cutin might therefore be taken to indicate other functions, such as defense against pathogens or protection from UV radiation, as suggested by Clarke and Robinson (2008), and warrants further investigation. We also note that the polymer suberin typically contains high amounts of aromatic monomers derived from cinnamic acid (Beisson et al., 2012) and suggest that the first pathways responsible for cutin synthesis in early diverging plants may have been the progenitors of suberin biosynthetic pathways in later diverging lineages.

The cutin polymer provides the major structural framework of the cuticle, but the wax that fills and covers this matrix is thought to contribute greatly to its sealing and protective properties, depending on both amount and composition (Yeats and Rose, 2013). Nonuniform deposition of waxes within the intra- and epicuticular regions of the cuticle is often observed and, together with the overall wax composition, leads to a diversity of epicuticular wax crystals and films (Jeffree, 2006). Analysis of *P. patens* waxes revealed four major compound classes: fatty alcohols, long-chain wax esters, VLCFAs, and alkanes (Figures 4A to 4D). In some plants, a particular compound class can account

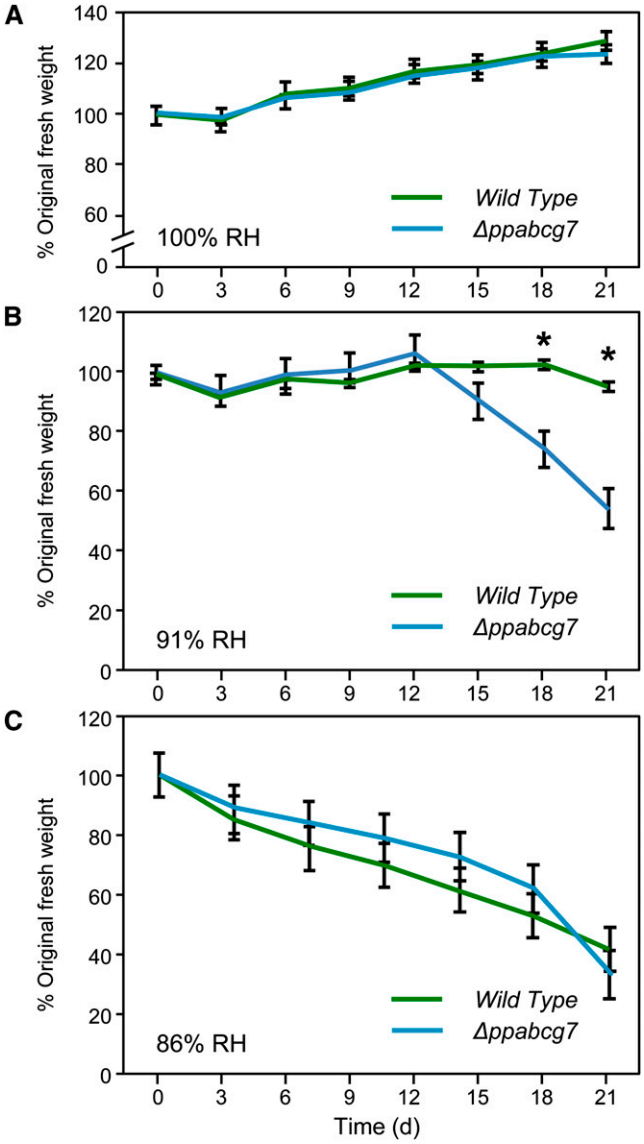

Figure 10. Response of Wild-Type and Mutant Moss Colonies to Desiccation Stress.

Fresh weight of wild-type and Δ*ppabcg7* moss colonies at 100% RH **(A)**, 91% RH **(B)**, and 86% RH **(C)** was measured over a 21-d period. Asterisks indicate statistically significant differences between wild-type and transgenic lines ($P < 0.05$, Student's *t* test). Error bars indicate SE; $3 \leq n \leq 5$.

for most of the cuticular wax, as with the fern *Pteridium aquilinum*, where wax esters comprise >90% of the surface wax load (Baker and Gaskin, 1987). In other species, such as *Arabidopsis*, the surface wax is composed of comparable amounts of several compound classes (Li-Beisson et al., 2010). It is clear that the bryophytes have the capacity to synthesize the full complement of wax compound classes mentioned, even though not all of them were found in *P. patens*. For example, the cuticular wax of the moss *Pogonatum urnigerum* has substantial amounts of secondary alcohols and related species produce long-chain aldehydes (Neinhuis and Jetter, 1995). Taken together, we suggest that the biosynthetic pathways needed to synthesize the diverse suite of cuticular waxes that have been identified in land plant lineages were likely present in the first land plant taxa, prior to the divergence of vascular plants. Moreover, specific evolutionary pressures have refined cuticular wax compositions resulting in the observed compositional and structural diversity.

The Cuticle Phenotype of Δ*ppabcg7* Suggests Deep Conservation of Cuticle-Associated Gene Pathways in Land Plants

Having establishing that the *P. patens* cuticle is architecturally and compositionally comparable to those of many later diverging plant lineages, we hypothesized that the underlying genetic pathways that regulate cuticle synthesis and assembly are likely also shared among land plants. To test this, we used the sequences of well-studied cuticle-associated genes in flowering plants to identify putative orthologs in the *P. patens* genome and indeed found that most of the gene families known to be involved in cuticle synthesis, trafficking, and assembly were represented. Among these genes was a putative ortholog (Pp-*ABCG7*) of the *Arabidopsis* ABCG transporters *ABCG11* (*WBC11*) and *ABCG12* (*WBC12*/*CER5*), which encode half transporters that form homo- or heterodimers and mediate the transport of waxes and cutin precursors across the plasma membrane (Kang et al., 2011). The *Arabidopsis abcg12* (*wbc12*) mutant has a 50% decrease in surface wax load and lipid inclusions in the vacuoles of the epidermal cells (Pighin et al., 2004), while the *abcg11* (*wbc11*) mutant phenotype is more severe, with a substantial reduction in levels of both cutin and wax, as well as severe dwarfing, a permeable cuticle, and postgenital organ fusions (Bird et al., 2007; Luo et al., 2007). A targeted knockout mutant of Pp-*ABCG7* (Δ*ppabcg7*) also showed a dwarf phenotype (Figure 7), accompanied by a substantial reduction in surface wax, while cutin levels were not affected (Figure 9). Furthermore, Δ*ppabcg7* had a reduced ability to tolerate low humidity conditions compared with the wild type (Figure 10B). The 91% RH conditions at which the reduced growth phenotype was apparent was selected because a study by Koster et al. (2010) indicated that wild-type *P. patens* is able to survive at this RH, but not lower. These conditions were therefore chosen as a tipping point at which impaired viability resulting from a defective cuticle might be more evident, as indeed proved to be the case.

The fact that no organ fusion phenotype or altered cuticle architecture was observed in Δ*ppabcg7* further suggests that ABCG7 is responsible for wax transport, as such phenotypes are more typically associated with cutin deficiency (Javelle et al., 2011). In addition, water loss through the cuticle is thought to be controlled mainly by wax composition and amount and is not correlated with cutin content (Burghardt and Riederer, 2006; Isaacson et al., 2009). We conclude that the physiological phenotypes of Δ*ppabcg7* are a consequence of its decreased cuticular wax content. The At-*abcg12* (At-*wbc12*) mutant shows lipidic inclusion bodies within the epidermal cells, presumably comprised of cuticular waxes that are unable to be transported out of the cell (Pighin et al., 2004). These were not observed in the epidermal cells of the Pp-*abcg7* mutant. It is possible that the moss cells have a feedback mechanism that prevents such waxes from accumulating in the cytoplasm or vacuole. Alternatively, the fact that Pp-*abcg7* was cultured under conditions approaching 100% humidity may have reduced the need for it to produce copious amounts of wax.

The reduction in the amount of cuticular wax, but not cutin, in Δ*ppabcg7*, together with the length of the predicted gene sequence, suggests that Pp-*ABCG7*, like At-*ABCG12* (At-*WBC12*), encodes a wax half transporter. In *Arabidopsis*, cuticle-associated half transporters dimerize in differing combinations to traffic different compound classes, and it is therefore likely that Pp-ABCG7 also forms either a homodimer or a heterodimer with another half transporter to traffic cuticular waxes. Due to these and other protein–protein interactions that may be necessary for the activity of this class of transporter, it is perhaps not surprising that Pp-*ABCG7* does not complement the At-*abcg12* mutant (see Supplemental Figure 3 online), since the precise protein conformations necessary for such interactions would likely not be conserved over the ~450 million years since the divergence of these species. Alternatively, constitutive expression of Pp-ABCG7 in the At-*abcg12* mutant driven by the 35S promoter may not be appropriate for its cell type–specific function, and use of an *Arabidopsis* epidermal-specific promoter might be sufficient for complementation. Another notable phenotype of Δ*ppabcg7* was the abnormal surface decorations of the spore walls (Figure 8). The *Arabidopsis* half transporter *ABCG26* is required for exine formation in pollen and is believed to be responsible for the export of sporopollenin precursors in tapetal cells (Kang et al., 2011). Our results suggest that ABCG7 may serve multiple functions in moss, depending on where it is expressed, or possibly with which other half transporter it dimerizes, and could play a role in both cuticle and spore wall formation.

Conclusions

The evolutionary origins of the molecular pathways that mediate cuticle biosynthesis and formation remain unclear, but it is likely that they were derived from those responsible for membrane lipid biosynthesis in the algal ancestors of the first land plants. An expansion of these new pathways in the first terrestrial plants into the complex cuticle biosynthetic machinery seen in angiosperms has been hypothesized for many years, but, until now, no concrete evidence has been presented. This study links cuticle formation in a bryophyte with one of its corresponding genetic pathways. The substantial reduction in cuticular wax in the Δ*ppabcg7* moss line suggests that the role of ABCG transporters in trafficking cuticle components has been conserved

since the earliest divergence of terrestrial plants. Taken together with the strong similarities in the chemical composition and structure between the *P. patens* cuticle and those of other diverse plant taxa, we conclude that at least some of the mechanisms required to synthesize a specialized lipidic cell wall have been conserved through plant evolution and were likely instrumental in allowing the first terrestrial plants to survive in desiccating environments.

METHODS

Plant Material and Cultivation

Wild-type *Physcomitrella patens* (Gransden 2008 strain, obtained from the Cold Spring Harbor Laboratory, NY) and mutant strains were cultured on BCDAT or BCD media (Nishiyama et al., 2000) supplemented with vancomycin (50 μg/mL) in 9-mm Petri plates overlaid with 9-mm-diameter cellophane discs (AA Packaging). Subcultures were performed by homogenizing protonemal material in water using a Power Gen 125 homogenizer (Fischer Scientific) or by placing small pieces of young protonemal tissue (<1 mm in diameter) on BCDAT plates to induce protonemal growth. To induce gametophore development, cellophane discs containing protonemal colonies were transferred to BCD medium without ammonium tartrate. Cultures were grown at 23°C under 120 μmol m^{-2} s^{-1} light with a long-day cycle (16 h light/8 h dark). Sporophytes were induced from gametophytes cultured in jiffy pots as described by Cove et al. (2009).

Light Microscopy

The phyllid transverse section depicted in Figure 1B was obtained from wild-type moss material fixed, embedded, and cryosectioned as described by Buda et al. (2009). A 6-μm cryosection was melted onto a VistaVision Histobond (VWR) slide, dried, and stained using safranin O (0.1% in 50% ethanol) with an alcian blue counterstain (0.1% in water). The slide was mounted in water and viewed using an AxioImager A1 microscope with an Achroplan ×20/0.45 objective and AxioCam Mrc color video camera (Zeiss) using differential interference contrast optics.

TEM

P. patens gametophores and sporophytes were fixed using conventional chemical protocols. Samples were fixed with 1% glutaraldehyde in 0.1 M Sorensen's phosphate buffer, postfixed in 1% osmium tetroxide, dehydrated in acetone, and embedded in Spurr's Low Viscosity Resin (EMS). Sections (60 to 80 nm) were cut using a diamond knife on a Reichert Om-U2 ultramicrotome (MOC), stained with uranyl acetate (1% in water) and lead citrate (0.1% in water), and viewed on a Libra 120 transmission electron microscope (Zeiss) at 120 kV, equipped with a Cantega G-2 camera (Olympus).

Scanning Electron Microscopy

Wild-type and Δ*ppabcg7* gametophores (at least 8 weeks old) were air dried overnight in a laminar flow hood, and individual phyllids were carefully dissected. These were sputter coated with gold-palladium for 90 s at 2.2 kV, and epicuticular wax crystals were imaged on a JEOL 6480 variable-pressure scanning electron microscope (JEOL) with secondary electrons at 15 kV with a spot size of 55. The wild-type moss spores depicted in Figure 8A were placed on nitrocellulose, plunge frozen in liquid nitrogen, and viewed on a JEOL 6480 variable-pressure scanning electron microscope with backscattered electrons under variable-pressure mode with 30 Pa of vacuum and a spot size of 60. Spores shown in Figure 8B and 8C were sputter coated for 50 s and visualized with secondary electrons at 10 to 12 kV and a spot size of 60.

Wax Analysis

Plates containing colonies of wild-type and Δ*ppabcg7* moss grown for 3 weeks on BCDAT medium, followed by 7 to 10 weeks on BCD medium, were opened for 2 h to reduce surface moisture. Colonies were then submerged for 30 s in a beaker of chloroform containing 150 μg each of methyl heptadecanoate, nonadecane, and heptadecanoic acid as internal standards. The extract was dried over anhydrous sodium sulfate, passed through filter paper, and concentrated using a rotary evaporator. Moss wax was prefractionated on preparative 20 × 20-cm TLC plates (Whatman; 250-μm coating, silica gel 60), using a mobile phase of 80:18:1 hexane:diethyl ether:glacial acetic acid and employing the sandwich technique, which consisted of a glass plate fastened to the TLC plate with a 1- to 2-mm space between it and the silica gel to allow for increased saturation of the atmosphere adjacent to the sample. Bands were visualized under a UV lamp after misting with primuline (0.005% in 80:20 acetone:water), scraped from the plate, and eluted from the silica with chloroform. The band extract corresponding to fatty acids and primary alcohols was derivatized using equal parts of bis-*N,O*-(trimethylsilyl)trifluoroacetamide and pyridine for 15 min at 100°C. All extracts were dried under a gentle stream of nitrogen and resuspended in chloroform. Wax compound identification was performed by GC-MS as described by Wang et al. (2011), using a 6890 gas chromatograph (Agilent) coupled to a GC Mate II mass spectrometer (JEOL). Individual waxes were quantified based on peak integration of the total ion chromatogram, except for wax esters, which were quantified using gas chromatography–flame ionization detection on a model 6850 gas chromatograph (Agilent) due to discrimination of the GC-MS against compounds in this molecular mass range. All waxes were quantified based on their corresponding internal standard, with the exception of primary alcohols, which were quantified using the heptadecanoic acid standard. AMDIS 32 GC-MS Analysis software (v 2.69) was used for peak identification and TSSPro GC-MS data reduction software (v 3.0) for manual peak integration.

Cutin Analysis

The same wild-type and Δ*ppabcg7* tissue that was extracted for wax analysis (see above) was oven-dried at 50°C for several days, and 4 g of dried tissue from each line was powdered in a pestle and mortar with liquid nitrogen and distributed among four tubes. The material was exhaustively delipidated as outlined by Li-Beisson et al. (2010) with the following modifications. All extraction steps were performed twice for 1 h each using a rotary shaker set to 300 rpm, and an additional two extractions with acetone were included after the last step. Base-catalyzed depolymerization, extraction, and subsequent trimethylsilyl derivatization of the samples were performed as described above. Extracts were resuspended in chloroform, and cutin monomers were identified by GC-MS. Individual monomers were quantified using ω-pentadecalactone as an internal standard with the software listed above.

Transient Expression and Subcellular Localization of Pp-ABCG7 in Onion Cells

The full-length coding sequence Pp-ABCG7 containing the *att* recombination sites (forward, 5′-GGGGACAAGTTTGTACAAAAAAGCAGGCTTCATGGCTTCTTCTAATTGTTTACATGC-3′, and reverse, 5′-GGGGACCACTTTGTACAAGAAAGCTGGGTCATCAATTGAAGTGAAATTAAAATTGTCA-3′) was synthesized (Life Technologies) and cloned into the pDONR221 vector by overnight incubation in the presence of Gateway BP clonase (Invitrogen) at 25°C, according to the manufacturer's

instructions. The positive entry clones were then introduced into the pSITE-4NA (RFP tag in the C terminus) destination vector (Chakrabarty et al., 2007). Plasma membrane labeling was based on the full-length coding region of At-PIP2A, a plasma membrane aquaporin, acquired from The Arabidopsis Information Resource Stock Center (ABRC stock numbers: CD3-1003; Cutler et al., 2000; Nelson et al., 2007) fused to the N terminus of GFP. Approximately 1 μg each of the PpABCG7-RFP and AtPIP2A-GFP plasmids was mixed and used to bombard onion (*Allium cepa*) epidermal cells as described by Yamane et al. (2005). The tissue was incubated for 16 to 24 h at 24°C in the dark, the epidermal layer was peeled, transferred to glass slides, and mounted in a 30% Suc solution to induce plasmolysis, and the cells were observed using a Leica TCS-SP5 confocal scanning laser microscope (Leica Microsystems).

ABCG Half Transporter Phylogenetic Analysis

Amino acid sequences of all known ABCG half transporters from *Arabidopsis thaliana* and *P. patens* were obtained from GenBank (http://www.ncbi.nlm.nih.gov) and Cosmoss (http://cosmoss.org) databases, respectively. Sequences were aligned using ClustalW (Thompson et al., 1994), and an unrooted neighbor joining phylogenetic tree was generated using MEGA5 software (Tamura et al., 2007) with bootstrap values assigned to each node (1000 replicates).

Δ*ppabcg7* Knockout Cassette Construction

To selectively disrupt *ABCG7*, the annotated gene sequence and surrounding genomic sequence were obtained from the latest version of the *P. patens* genome using the BLAST tool in the Cosmoss database. Primer pair PpABCG7-5FR (see Supplemental Table 1 online) incorporating the *Hin*dIII and *Eco*RI restriction sites was used to amplify the 5′ flanking region (1157 bp) of *ABCG7*. Similarly, primer pair PpABCG7-3FR (see Supplemental Table 1 online) incorporating the *Bam*HI and *Sac*I restriction sites was used to amplify the 3′ flanking region (1143 bp) of the target gene using ExTaq PCR (Takara). These flanking regions were subsequently cloned into the pTN80 vector (obtained from Mitsuyasu Hasebe at the National Institute for Basic Biology, Okazaki, Japan) on either side of the *nptII* selectable marker. The Pp-*ABCG7* knockout cassette was then replicated in *Escherichia coli*, isolated, and linearized using the *Bss*HII restriction enzyme prior to moss transformation.

Transformation to Generate Δ*ppabcg7*

Polyethylene glycol–mediated protoplast transformation was performed as outlined by Cove et al. (2009) and Saavedra et al. (2011). Colonies surviving the first round of selection on BCDAT medium supplemented with G418 were maintained for 1 week on BCDAT without antibiotics and then subjected to a second round of selection on BCDAT with G418 for 1 week. Several surviving colonies were propagated and screened using PCR primers specific to both Pp-*ABCG7* and the *nptII* resistance marker (Figures 6A and 6B; see Supplemental Table 1 online) to verify correct targeting of the knockout cassette.

Expression Analysis

Total mRNA was isolated from moss protonema (2 weeks old) and gametophores (8 weeks old) using the Dynabead mRNA direct kit (Invitrogen Dynal) following the manufacturer's instructions. One hundred micrograms of purified mRNA was used for subsequent cDNA synthesis using Superscript II (Invitrogen) and according to the manufacturer's instructions. The gene-specific PCR primer pair PpABCG7-3FR (see Supplemental Table 1 online) was used to amplify a 221-bp fragment at the 3′ end of the mature mRNA of *ABCG7*. The protonema and gametophore cDNA libraries of the wild-type and Δ*ppabcg7* lines were screened with these primers via PCR (94°C for 5 min; 94°C for 30 s, 54°C for 45 s, and 72°C for 30 s for 38 cycles) to determine presence or absence of gene expression. PCR primers designed to the 3′ end of *Act2* mRNA (primer pair PpACT2; see Supplemental Table 1 online) were used as a positive control for gene expression between tissue types and genetic lines (Huang et al., 2009).

Physiological Assays

For the physiological studies of wild-type and Δ*ppabcg7* moss grown under different RHs, cultures were initiated using three pieces of protonemal tissue (<1 mm in diameter) placed on a plate of BCDAT media supplemented with vancomycin (50 μg/μL) and overlaid with cellophane (AA Packaging). After 3 weeks, the 9-mm cellophane discs were transferred to BCD media for an additional 3 weeks to induce robust gametophore growth. Wild-type and Δ*ppabcg7* cultures were weighed (cellophane and moss colonies only), placed onto plates containing BCD media, and exposed to different RH conditions. The plates were left open inside sealed chambers (Pyrex dishes) floating on solutions of saturated magnesium sulfate or potassium chloride to obtain RHs of 91 or 86%, respectively (Koster et al., 2010). Other moss cultures were sealed in plates containing BCD media supplemented with vancomycin (50 μg/μL) to generate close to 100% RH. The fresh weight of each sample (cellophane and moss colonies) was recorded every 3 d for 3 weeks. After 3 weeks, the final weight was recorded and the mass of the cellophane was subtracted from each previous measurement of the sample to obtain fresh weight values. Any plates with substantial microbial contamination were discarded and were not included in subsequent statistical analyses.

Complementation of At-abcg12 with PPABCG7

To construct the plasmid vector for complementation analysis, the Pp-*ABCG7* coding sequence (as described above) was cloned into the pDONR Gateway shuttle vector and then subcloned in frame with the *Pro35S*:*CPMV 5′-UTR* in the destination vector pEAQ-HT-DEST1. The vector construct was transformed into 3-week-old *abcg12* T-DNA insertional mutant *Arabidopsis* plants (Salk 036776) by *Agrobacterium tumefaciens*–mediated transformation (GV2260 strain) as previously described (Clough and Bent, 1998). To identify transformants, the T1 seeds were sown on one-quarter Murashige and Skoog plates containing 100 mg/L kanamycin and screened by PCR using Pp-*ABCG7*–specific primers (primer pair PpABCG7-S; see Supplemental Table 1 online). Offspring from a transformed line (a segregating T2 population) were grown and genotyped by PCR for the presence of the *ABCG7* transgene. Inflorescence stems were collected from five transgenic and three nontransgenic T2 plants, as well as from three wild-type plants, grown concurrently. The stems, from which leaves, flowers, and siliques were removed, were cut into 3-cm sections, with eight to 15 sections collected per plant, and sections from each plant were swirled in 30 mL of chloroform, containing 100 μL of tetracosane as an internal standard, for 30 s. The diameters of the stem sections were measured at their center to calculate surface area. Wax extracts were dried over anhydrous sodium sulfate, filtered, and then concentrated to a volume of 4 mL. The level of C_{29} alkane in these samples was quantified as described above.

Accession Numbers

Sequence data from this article can be found in the GenBank/EMBL data libraries under the following accession numbers: XP_001775949 (Pp-*ABCG7* genomic sequence), XP_001775897 (Pp-*ABCG7* mRNA sequence), and XM_001775900 (Pp-*ACT2* mRNA sequence).

Supplemental Data

The following materials are available in the online version of this article.

Supplemental Figure 1. Localization of Pp-ABCG7 Fused to an RFP Marker Protein Using Confocal Scanning Laser Microscopy, following Transient Expression in Onion Epidermal Cells.

Supplemental Figure 2. Abnormal Sporophyte Phenotype of Δ*ppabcg7*.

Supplemental Figure 3. Overexpression of Pp-*ABCG7* in the *Arabidopsis abcg12* Mutant.

Supplemental Table 1. List of PCR Primers, Referenced in Methods.

Supplemental Data Set 1. Protein Alignment of All Known ABCG Half Transporters from *Arabidopsis* and *P. patens.*

ACKNOWLEDGMENTS

We thank Antonio Matas for helpful discussion and for assisting with the statistical analysis, Eliel Ruiz-May for assistance with confocal microscopy, and Iben Sørensen for careful reading of the article. This work was supported by grants from the National Science Foundation (Plant Genome Program, DBI-0606595), by the U.S.–Israel Binational Agricultural Research and Development Fund (IS-4234-09), and by the Agriculture and Food Research Initiative Competitive Grants Program (2011-67013-19399) from the USDA National Institute of Food and Agriculture. G.J.B. and T.H.Y. were partly supported by a National Institutes of Health chemistry/biology interface training grant (T32 GM008500).

AUTHOR CONTRIBUTIONS

G.J.B. designed and performed the research, analyzed data, and cowrote the article. W.J.B., E.A.F., S.P., T.H.Y., L.Z., and D.S.D. performed the research and analyzed data. J.K.C.R. designed the research, analyzed data, and cowrote the article.

Received August 19, 2013; revised September 11, 2013; accepted September 25, 2013; published October 25, 2013.

REFERENCES

Baker, E.A., and Gaskin, R.E. (1987). Composition of leaf epicuticular waxes of *Pteridium* subspecies. Phytochemistry **26:** 2847–2848.

Barthlott, W., and Neinhuis, C. (1997). Purity of the sacred lotus, or escape from contamination in biological surfaces. Planta **202:** 1–8.

Beerling, D.J., and Franks, P.J. (2009). Evolution of stomatal function in 'lower' land plants. New Phytol. **183:** 921–925.

Beisson, F., Li-Beisson, Y., and Pollard, M. (2012). Solving the puzzles of cutin and suberin polymer biosynthesis. Curr. Opin. Plant Biol. **15:** 329–337.

Bird, D., Beisson, F., Brigham, A., Shin, J., Greer, S., Jetter, R., Kunst, L., Wu, X., Yephremov, A., and Samuels, L. (2007). Characterization of *Arabidopsis* ABCG11/WBC11, an ATP binding cassette (ABC) transporter that is required for cuticular lipid secretion. Plant J. **52:** 485–498.

Buda, G.J., Isaacson, T., Matas, A.J., Paolillo, D.J., and Rose, J.K. C. (2009). Three-dimensional imaging of plant cuticle architecture using confocal scanning laser microscopy. Plant J. **60:** 378–385.

Budke, J.M., Goffinet, B., and Jones, C.S. (2011). A hundred-year-old question: Is the moss calyptra covered by a cuticle? A case study of *Funaria hygrometrica*. Ann. Bot. (Lond.) **107:** 1279–1286.

Burghardt, M., and Riederer, M. (2006). Cuticular transpiration. In Biology of the Plant Cuticle, M. Riederer and C. Muller, eds (Oxford, UK: Blackwell Publishing), pp. 292–311.

Caldicott, A.B., and Eglinton, G. (1976). Cutin acids from bryophytes: An ω-1 hydroxy alkanoic acid in two liverwort species. Phytochemistry **15:** 1139–1143.

Caldicott, A.B., Simoneit, B.R.T., and Eglinton, G. (1975). Alkanetriols in psilotophyte cutins. Phytochemistry **14:** 2223–2228.

Chakrabarty, R., Banerjee, R., Chung, S.M., Farman, M., Citovsky, V., Hogenhout, S.A., Tzfira, T., and Goodin, M. (2007). PSITE vectors for stable integration or transient expression of autofluorescent protein fusions in plants: Probing *Nicotiana benthamiana*-virus interactions. Mol. Plant Microbe Interact. **20:** 740–750.

Charron, A.J., and Quatrano, R.S. (2009). Between a rock and a dry place: The water-stressed moss. Mol. Plant **2:** 478–486.

Clarke, L.J., and Robinson, S.A. (2008). Cell wall-bound ultraviolet-screening compounds explain the high ultraviolet tolerance of the Antarctic moss, *Ceratodon purpureus*. New Phytol. **179:** 776–783.

Clayton-Greene, K.A., Collins, N.J., Green, T.G.A., and Proctor, M.C.F. (1985). Surface wax, structure and function in leaves of Polytrichaceae. J. Bryol. **13:** 549–562.

Clough, S.J., and Bent, A.F. (1998). Floral dip: A simplified method for Agrobacterium-mediated transformation of Arabidopsis thaliana. Plant J. **16:** 735–743.

Cove, D., Bezanilla, M., Harries, P., and Quatrano, R. (2006). Mosses as model systems for the study of metabolism and development. Annu. Rev. Plant Biol. **57:** 497–520.

Cove, D.J., Perroud, P., Charron, A.J., McDaniel, S.F., Khandelwal, A., and Quatrano, R.S. (2009). The moss *Physcomitrella patens*: A novel model system for plant development and genomic studies. In Emerging Model Organisms, Vol. 1, (Cold Spring Harbor, NY: Cold Spring Harbor Laboratory Press), pp. 69–104.

Cutler, S.R., Ehrhardt, D.W., Griffitts, J.S., and Somerville, C.R. (2000). Random GFP:cDNA fusions enable visualization of subcellular structures in cells of *Arabidopsis* at a high frequency. Proc. Natl. Acad. Sci. USA **97:** 3718–3723.

Das, S., and Thakur, S. (1989). Constituent acids of *Limonia acidissima* leaf cutin. Phytochemistry **28:** 509–511.

Duckett, J.G., Pressel, S., P'ng, K.M.Y., and Renzaglia, K.S. (2009). Exploding a myth: The capsule dehiscence mechanism and the function of pseudostomata in *Sphagnum*. New Phytol. **183:** 1053–1063.

Haas, K. (1982). Surface wax of *Andreaea* and *Pogonatum* species. Phytochemistry **21:** 657–659.

Hohe, A., Egener, T., Lucht, J.M., Holtorf, H., Reinhard, C., Schween, G., and Reski, R. (2004). An improved and highly standardised transformation procedure allows efficient production of single and multiple targeted gene-knockouts in a moss, *Physcomitrella patens*. Curr. Genet. **44:** 339–347.

Holloway, P.J. (1982). The chemical constitution of plant cutins. In The Plant Cuticle, D.F. Cutler, K.L. Alvin, and C.E. Price, eds (London, UK: Academic Press), pp. 45–85.

Holloway, P.J., Deas, A.H.B., and Kabaara, A.M. (1972). Composition of cutin from coffee leaves. Phytochemistry **11:** 1443–1447.

Hunneman, D.H., and Eglinton, G. (1972). The constituent acids of gymnosperm cutins. Phytochemistry **11:** 1989–2001.

Huang, C.Y., Chung, C.I., Lin, Y.C., Hsing, Y.I., and Huang, A.H.C. (2009). Oil bodies and oleosins in *Physcomitrella* possess characteristics representative of early trends in evolution. Plant Physiol. **150:** 1192–1203.

Isaacson, T., Kosma, D.K., Matas, A.J., Buda, G.J., He, Y., Yu, B., Pravitasari, A., Batteas, J.D., Stark, R.E., Jenks, M.A., and Rose, J.K.C. (2009). Cutin deficiency in the tomato fruit cuticle consistently affects resistance to microbial infection and biomechanical properties, but not transpirational water loss. Plant J. **60:** 363–377.

Javelle, M., Vernoud, V., Rogowsky, P.M., and Ingram, G.C. (2011). Epidermis: The formation and functions of a fundamental plant tissue. New Phytol. **189:** 17–39.

Jeffree, C.E. (2006). The fine structure of the plant cuticle. In Biology of the Plant Cuticle, M. Riederer and C. Muller, eds (Oxford, UK: Blackwell Publishing), pp. 11–125.

Jetter, R., Kunst, L., and Samuels, A.L. (2006). Composition of plant cuticular waxes. In Biology of the Plant cuticle, M. Riederer and C. Muller, eds (Oxford, UK: Blackwell Publishing), pp. 145–181.

Kang, J., Park, J., Choi, H., Burla, B., Kretzschmar, T., Lee, Y., and Martinoia, E. (2011). Plant ABC transporters. The Arabidopsis Book **9:** e0153, doi/10.1199/tab.0153.

Koster, K.L., Balsamo, R.A., Espinoza, C., and Oliver, M.J. (2010). Desiccation sensitivity and tolerance in the moss *Physcomitrella patens*: Assessing limits and damage. Plant Growth Regul. **62:** 293–302.

Leide, J., Hildebrandt, U., Reussing, K., Riederer, M., and Vogg, G. (2007). The developmental pattern of tomato fruit wax accumulation and its impact on cuticular transpiration barrier properties: Effects of a deficiency in a β-ketoacyl-coenzyme A synthase (LeCER6). Plant Physiol. **144:** 1667–1679.

Li-Beisson, Y., et al. (2010). Acyl-lipid metabolism. The Arabidopsis Book **8:** e0133, doi/10.1199/tab.0133.

Luo, B., Xue, X.Y., Hu, W.L., Wang, L.J., and Chen, X.Y. (2007). An ABC transporter gene of *Arabidopsis thaliana*, *AtWBC11*, is involved in cuticle development and prevention of organ fusion. Plant Cell Physiol. **48:** 1790–1802.

Matas, A.J., et al. (2011). Tissue- and cell-type specific transcriptome profiling of expanding tomato fruit provides insights into metabolic and regulatory specialization and cuticle formation. Plant Cell **23:** 3893–3910.

Minami, A., Nagao, M., Ikegami, K., Koshiba, T., Arakawa, K., Fujikawa, S., and Takezawa, D. (2005). Cold acclimation in bryophytes: low-temperature-induced freezing tolerance in *Physcomitrella patens* is associated with increases in expression levels of stress-related genes but not with increase in level of endogenous abscisic acid. Planta **220:** 414–423.

Neinhuis, C., and Jetter, R. (1995). Ultrastructure and chemistry of epicuticular wax crystals in Polytrichales sporophytes. J. Bryol. **18:** 399–406.

Nelson, B.K., Cai, X., and Nebenführ, A. (2007). A multicolored set of *in vivo* organelle markers for co-localization studies in *Arabidopsis* and other plants. Plant J. **51:** 1126–1136.

Nishiyama, T., Hiwatashi, Y., Sakakibara, I., Kato, M., and Hasebe, M. (2000). Tagged mutagenesis and gene-trap in the moss, *Physcomitrella patens* by shuttle mutagenesis. DNA Res. **7:** 9–17.

Nissinen, R., and Sewón, P. (1994). Hydrocarbons of *Polytrichum commune*. Phytochemistry **37:** 179–182.

Pighin, J.A., Zheng, H., Balakshin, L.J., Goodman, I.P., Western, T.L., Jetter, R., Kunst, L., and Samuels, A.L. (2004). Plant cuticular lipid export requires an ABC transporter. Science **306:** 702–704.

Post-Beittenmiller, D. (1998). The cloned *Eceriferum* genes of *Arabidopsis* and the corresponding *Glossy* genes in maize. Plant Physiol. Biochem. **36:** 157–166.

Proctor, M.C.F. (1979). Surface wax on the leaves of some mosses. J. Bryol. **10:** 531–538.

Rautengarten, C., Ebert, B., Ouellet, M., Nafisi, M., Baidoo, E.E.K., Benke, P., Stranne, M., Mukhopadhyay, A., Keasling, J.D., Sakuragi, Y., and Scheller, H.V. (2012). Arabidopsis *Deficient in Cutin Ferulate* encodes a transferase required for feruloylation of ω-hydroxy fatty acids in cutin polyester. Plant Physiol. **158:** 654–665.

Reina-Pinto, J.J., and Yephremov, A. (2009). Surface lipids and plant defenses. Plant Physiol. Biochem. **47:** 540–549.

Rensing, S.A., et al. (2008). The *Physcomitrella* genome reveals evolutionary insights into the conquest of land by plants. Science **319:** 64–69.

Saavedra, L., Balbi, V., Lerche, J., Mikami, K., Heilmann, I., and Sommarin, M. (2011). PIPKs are essential for rhizoid elongation and caulonemal cell development in the moss *Physcomitrella patens*. Plant J. **67:** 635–647.

Sack, F.D., and Paolillo, D.J. (1983). Stomatal pore and cuticle formation in *Funaria*. Protoplasma **116:** 1–13.

Samuels, L., Kunst, L., and Jetter, R. (2008). Sealing plant surfaces: Cuticular wax formation by epidermal cells. Annu. Rev. Plant Biol. **59:** 683–707.

Schönherr, J., and Ziegler, H. (1975). Hydrophobic cuticular ledges prevent water entering the air pores of liverwort thalli. Planta **124:** 51–60.

Shepherd, T., and Wynne Griffiths, D. (2006). The effects of stress on plant cuticular waxes. New Phytol. **171:** 469–499.

Tamura, K., Dudley, J., Nei, M., and Kumar, S. (2007). MEGA4: Molecular Evolutionary Genetics Analysis (MEGA) software version 4.0. Mol. Biol. Evol. **24:** 1596–1599.

Thompson, J.D., Higgins, D.G., and Gibson, T.J. (1994). CLUSTAL W: Improving the sensitivity of progressive multiple sequence alignment through sequence weighting, position-specific gap penalties and weight matrix choice. Nucleic Acids Res. **22:** 4673–4680.

Wang, Z., Guhling, O., Yao, R., Li, F., Yeats, T.H., Rose, J.K.C., and Jetter, R. (2011). Two oxidosqualene cyclases responsible for biosynthesis of tomato fruit cuticular triterpenoids. Plant Physiol. **155:** 540–552.

Wood, A.J. (2005). Eco-physiological adaptations to limited water environments. In Plant Abiotic Stress, M.A. Jenks and P.M. Hasegawa, eds (Oxford, UK: Blackwell Publishing), pp. 1–13.

Wyatt, H.D.M., Ashton, N.W., and Dahms, T.E.S. (2008). Cell wall architecture of *Physcomitrella patens* is revealed by atomic force microscopy. Botany **86:** 385–397.

Yamane, H., Lee, S.-J., Kim, B.-D., Tao, R., and Rose, J.K.C. (2005). A coupled yeast signal sequence trap and transient plant expression strategy to identify genes encoding secreted proteins from peach pistils. J. Exp. Bot. **56:** 2229–2238.

Yeats, T.H., Buda, G.J., Wang, Z., Chehanovsky, N., Moyle, L.C., Jetter, R., Schaffer, A.A., and Rose, J.K.C. (2012). The fruit cuticles of wild tomato species exhibit architectural and chemical diversity, providing a new model for studying the evolution of cuticle function. Plant J. **69:** 655–666.

Yeats, T.H., and Rose, J.K.C. (2013). The formation and function of plant cuticles. Plant Physiol. **163:** 5–20.